AIIM

Association for Information and Image Management

1100 Wayne Avenue, Suite 1100
Silver Spring, Maryland 20910

301/587-8202

Centimeter

Inches

MANUFACTURED TO AIIM STANDARDS
BY APPLIED IMAGE, INC.

1 of 1

Conf-941142--2-
Pt.1

LA-UR- 94- 724
TSA-6-94-R105

Los Alamos National Laboratory is operated by the University of California for the United States Department of Energy under contract W-7405-ENG-36

TITLE: NONLINEAR ASPECTS OF HIGH HEAT FLUX NUCLEATE BOILING HEAT TRANSFER
Part I: Formulation

AUTHOR(S): Pratap Sadasivan
Cetin Unal
Ralph Nelson

SUBMITTED TO: 1994 ASME Winter Meeting
November 13–18, 1994
Chicago, Il

Los Alamos
Los Alamos National Laboratory
Los Alamos, New Mexico 87545

NONLINEAR ASPECTS OF HIGH HEAT FLUX NUCLEATE BOILING HEAT TRANSFER —Part I: Formulation

Pratap Sadasivan, Cetin Unal, and Ralph Nelson

Los Alamos National Laboratory
Technology and Safety Assessment Division
Safety Assessment Group
Los Alamos, NM 87545

This paper outlines the essential details of the formulation and numerical implementation of a model used to study nonlinear aspects of the macrolayer-controlled heat transfer process associated with high heat flux nucleate boiling and the critical heat flux. The model addresses the three-dimensional transient conduction heat transfer process within the problem domain comprised of the macrolayer and heater. Heat dissipation from the heater is modeled as the sum of transient transport into the macrolayer, and the heat loss resulting from evaporation of menisci associated with vapor stems.

INTRODUCTION

Mechanistic prediction of nucleate boiling and critical heat fluxes in even the most simple configurations has eluded researchers despite decades of efforts. In the absence of mechanistic predictive capability, a plethora of empirical correlations has been proposed for various boiling configurations. Typically each correlation is applicable only in a narrow range of experimental conditions. There is as yet no consensus as to what the relevant independent variables are. As a result, different empirical correlations for the same experimental condition do not necessarily all contain the same independent variables. And even for correlations within a data set, the best optimized correlation typically exhibits a considerably broad error band for that data set itself.

For a number of years, the normal tendency was to attribute scatter to "nuisance variables" such as surface aging, etc. However, recently Dhir (1990) suggested that a renewed effort in the study of the boiling process should be undertaken with both experimental and modeling efforts. Dhir further suggested that while there are numerous subprocesses involved in boiling, one key issue was the "... density of active nucleation sites and the relation between active cavities and the cavities that are formed on the surface after the surface is prepared by following a certain procedure." Somewhat along the same line of reasoning, Kenning (1992) raised the question as to whether mechanistic modeling efforts thus far have overlooked one or more key characteristic of the boiling system. Kenning suggested the issue of spatial and temporal temperature variations on the heater surface as one possibility. While these two points may appear to be unrelated, we interpret them as being the same issue—the activation and deactivation on nucleate sites that produce and are caused by spatial thermal distributions on the heater surface.

With recent advances in the studies of nonlinear dynamic systems and the demonstration that even simple systems could generate "noisy" results, it would appear prudent to attempt to better understand if a possible source of the data scatter could be nonlinear dynamic effects. Transient on-off behavior of other systems has been shown to lead to nonlinear and even chaotic behavior. For example, it has been shown that nonlinear effects displayed by the driven diode resonator circuit shown in Fig. 1 can be attributed to the on-off behavior of the diode in the circuit [Moon (1987)]. Thus, it is the objective of the present study is to investigate whether the on-off behavior of nucleation sites, as a result of the feedback between the surface temperature patterns and the individual sites, can introduce nonlinear effects into the boiling system that could also explain some of the data scatter.

Some previous studies on thermal interactions

Pasamehmetoglu and Nelson (1991) examined the influence of non-uniformities of site distribution on the characteristics in low heat flux boiling (isolated bubble region). They found that thermal interactions among sites as a result of nonuniform site distributions can cause fairly significant spatial variations in surface temperature. Experimental evidence of interaction between nucleation sites has been provided by several earlier studies [for example, Chekanov (1977),

Calka and Judd (1985), and Sultan and Judd (1983)]. Such nonlinear effects could be partly responsible for the data scatter commonly seen in boiling experiments.

Kenning (1990, 1992) used liquid crystal thermography to map the temperature patterns on the surface of thin stainless steel heaters during low flux nucleate boiling (isolated bubble region). Variations in heater surface superheat of as much as 150% of the mean value were observed in some experiments. The liquid crystal images present a detailed map of the spatial temperature patterns on the heater surface; the images were taken at intervals of 10 s, so that information on the temporal variations was limited. However, even this limited data on temporal variations revealed that many nucleation sites on the surface activate rather intermittently.

Numerical experimentation or "modeling philosophy"

Before we discuss the model, a few additional explanatory remarks about the approach used in this study would be in order. This study is currently *not* aimed at predicting nucleate boiling or the critical heat flux. In other words, the model is currently not a predictive tool. The model has been developed as a means of exploring boiling. What it attempts to do is mimic the behavior of a real surface in nucleate boiling. Mimicking the behavior of an actual system does not mean that it will enable us to predict the behavior of the system; it merely presents us with a means to explore possible characteristics of the system to understand better the effects of particular processes and their potential interaction.

We will term this approach numerical experimentation. Numerical experimentation might be defined as sensitivity studies that investigate the influence of basic physical phenomena as opposed to the influence of a given quantity upon a single physical phenomenon. We would hope the results of such studies might either identify future experiments to clarify dominant phenomena or focus future mechanistic modeling efforts.

The model of Pasamehmetoglu et al. (1993) has been adapted to undertake the three-dimensional study of the transient activation and deactivation of multiple sites under a single mushroom bubble in the high heat-flux nucleate boiling region. Toward this end, a supercomputer analysis code, MACRO3D, has been developed. MACRO3D is a three-dimensional finite-volume conduction

analysis code that can simulate the conduction process in the combined heater-liquid macrolayer domain. It contains a number of provisions to incorporate realistic experimental conditions in the simulation. This paper describes the essential details of the model and its numerical implementation. Results obtained using the study are discussed in a companion paper.

Currently, the model includes several key assumptions. It may be argued that such assumptions render the model and computer code unsubstantiated and invalid. Such an argument would be valid if the model and code were being presented as predictive tools. However, as we have stated already, the model used in this study is, in its current form, not a predictive tool. Therefore, it is impossible to validate MACRO3D in the manner in which predictive computer codes are traditionally validated—comparing numerical predictions with experimental data. In the context of MACRO3D, validation is merely to ensure that the numerics of the code are correct; details of such validation will be described in this paper.

HEAT TRANSFER MODEL

The basic configuration to be studied is pool boiling on a flat horizontal surface. The fluid is water, so that in the high heat flux range, a number of mushroom bubbles would be located on the heater surface. Due to the extremely large number of sites that would be active under each bubble, we have chosen to consider only a segment of the heater under one of the bubbles. Enough sites are included within the heater segment considered to allow the segment to be representative of the region under the bubble. This configuration provides an additional advantage in that it eliminates the behavior of the individual bubbles that exists in the discrete bubble region and allows us to study the thermal interaction of a number of sites all exposed to identical hydraulic conditions. For clarity of illustration, an axisymmetric configuration with one single vapor stem located at an active nucleation site is shown concentric with a circular heater section in Fig. 2. In practice, MACRO3D represents a heater segment with many potential sites available. It tracks the transient development of the temperature distributions in both the heater and macrolayer over successive bubble hovering periods.

Governing equation

We define the domain of interest to be that set of points {x, y, z} within the heater-macrolayer composite domain. The top and bottom surfaces of the heater and macrolayer will be limited to flat planes. The thickness of the heater is denoted by H, and the thickness of the macrolayer is denoted by δ, so that $0 \le z \le H+\delta$. The heater is bounded by the surface set defined as $\{S_t, S_b, S_s\}$, where S_t denotes the top surface, S_b, the bottom surface, and S_s, the side surface. Similarly the top surface of the macrolayer is denoted by S_{mt} and the vertical walls of vapor stems in the macrolayer are denoted by $S_{mv,i}$, where i denotes the number of the site associated with the stem.

The governing equation for the combined heater-macrolayer region can be written as

$$\text{Div}\,(k\ \text{grad}\,T) + \zeta q''' = \frac{\partial}{\partial t}\left[\rho\, C_p\, T\right] . \tag{1}$$

If the heat is generated by ohmic heating, ζ=1. If the heat flux is imposed externally, ζ=0 and the heat flux is included as a boundary condition on the bottom surface of the heater. Within the liquid macrolayer, ζ=0. The composite region can be handled by treating it as a region with variable properties, i.e., the properties of the heater material are used for $0 \le z \le H$, and those of the liquid are used for $H < z \le H+\delta$. Pasamehmetoglu et al. (1993) provide a detailed discussion of Eq. (1) compared to other modeling approaches.

When the temperature variations on and within the domain are small, the thermal properties can be assumed independent of temperature so that Eq. 1 can be written as

$$\frac{\partial T}{\partial t} - \frac{k}{\rho C_p}\left[\frac{\partial^2 T}{\partial x^2} + \frac{\partial^2 T}{\partial y^2} + \frac{\partial^2 T}{\partial z^2}\right] = \frac{\zeta q'''}{\rho C_p} \tag{2}$$

for all {x, y, z, t}.

Activation and deactivation of cavities

It is assumed that cavity activation can occur at any time. Currently we assume that once a cavity is activated, the triple interface contact line associated with the

site moves outside the cavity instantaneously—that is, the vapor stem associated with the site is formed immediately. This is expected to be a reasonable assumption at high heat flux levels because the waiting time for the mushroom bubbles is on the order of 1 to 3 ms so that formation of the stems themselves should be much less. We also assume that the size of the stem is a uniform multiple of the corresponding cavity size. In the present study we assume that the diameter of the vapor stem is ten times that of the site that originated it.

Once the stem is formed outside the cavity, meniscus evaporation causes fairly significant local cooling near the site. Experimental evidence of this is provided by the liquid crystal photographs of Kenning (1992) for low heat flux levels. The local cooling in turn decreases the local superheat at the cavity, and the temperature could drop to levels below the deactivation temperature. We assume that this drop in temperature does not immediately cause the stem to deactivate. This is based on the fact that the triple-phase contact line is located outside the site and is unaffected by what happens at the cavity that originated it. This assumption appears reasonable because a meniscus once formed can remain stable as long as there is sufficient liquid available in the macrolayer to support it. Upon departure of the overlying mushroom bubble, however, the resupply of fresh liquid from the bulk removes existing menisci on the surface, and new stems are generated at cavities that satisfy the activation criterion. Therefore, if a site active during the previous period has cooled down to a temperature below its deactivation superheat, it will not automatically activate at the beginning of the succeeding period.

The top surface of the heater, S_t, has N potential nucleation sites located on it. Figure 3 shows the typical geometry of a small segment of the heater top surface. Each site has a cavity associated with it that controls site activation and deactivation. Let R_c denote the cavity region on S_t and g(x,y,H) represent a function defining the cavity perimeter. The perimeter length of the i-th cavity is given by

$$L_{c,i} = \int_{g_i} dl \ . \tag{3}$$

We will assume that the cavity activation is defined as the cavity temperature required as a function of its size. A site activates if the temperature at that site

exceeds its activation temperature. Several equations have been proposed to relate the size of a cavity and the superheat required to activate it. Griffith and Wallis (1960) obtained the following equation from a thermodynamic analysis:

$$r_c = \frac{2\sigma T_{sat}}{\rho_g h_{fg}(T_w - T_{sat})} \quad . \tag{4}$$

Hsu (1962) obtained the following equation for the size range of active cavities at a given wall superheat:

$$r_c = \frac{\delta_{th}\left(T_w - T_{sat}\right)}{2C_1(T_w - T_\infty)} \pm \sqrt{1 - 8\frac{C_1}{C_2}\frac{(T_w - T_\infty)T_{sat}\sigma}{\left(T_w - T_{sat}\right)\delta_{th}\rho_g h_{fg}}} \quad , \tag{5}$$

where C_1 and C_2 are constants with values 2. 0 and 1.25, respectively, and δ_{th} is the thickness of the thermal layer. The most favorable cavity to be activated at a given superheat is obtained from Eq. (5) as

$$r_c = \frac{3.2\sigma T_{sat}}{\rho_g h_{fg}\left(T_w - T_{sat}\right)} \quad . \tag{6}$$

The predicted superheat-radius relationship calculated from Eq. (6) is in fair agreement with the lower bound of the range predicted by Eq. (5). Thus, we use Eq. (6) as the activation criterion.

Because we will initially assume circular cavities, the perimeter length is related to the radius and we can write the cavity activation temperature as related to the perimeter. For the i-th cavity, the activation temperature can be written as

$$T_{act,i} = T_{act}(L_{c,i}) = T_{sat} + \frac{3.2\,\sigma\, T_{sat}}{\rho_g\, h_{fg}\,(L_{c,i}/2\pi)} \quad . \tag{7}$$

Although the deactivation is commonly recognized to be less than the activation temperature [see Kenning (1992)], no predictive expression similar to Eqs. (4) and (5) is currently available. In the present study, we assume that the deactivation temperature for any site is 5°C below its activation temperature. Thus,

$$T_{deact,i} = T_{deact}(L_{c,i}) = T_{act,i} - 5.0 \quad . \tag{8}$$

Sites that are not activated are treated as any other macrolayer covered region on the heater surface, S_t, and transport heat into the macrolayer above them by conduction.

Vapor stems

Once activated, each cavity site has a vapor stem associated with it. Let R_s denote the region contained within an active site's vapor-stem base and f represent the function defining its perimeter. This is shown in Fig. 3. In general, once a nucleation cavity is activated, the formation of the vapor stem is a dynamic process, i.e., $R_s(t)$ and $f(x,y,H,t)$. We will neglect this growth and assume the vapor stem is represented by a static position, i.e., R_s and $f(x,y,H)$.

The perimeter of the i-th vapor stem is given by

$$L_{s,i} = \int_{f_i} dl \quad . \tag{9}$$

The region around the vapor-stem base where meniscus evaporation takes place is denoted as R_e. The resulting evaporative area for the i-th vapor-stem can be written as

$$A_{e,i} = \int_{w_i}^{f_i} da \quad , \tag{10}$$

where f_i is assumed to represent the outside of the annular evaporative region and w_i defines the inside. As noted earlier, we assume that the diameter of the vapor stem is ten times that of the cavity or $L_{s,i} = 10\, L_{c,i}$.

Boundary conditions

Boundary conditions will be divided into those applied to the heater and those applied to the liquid macrolayer. Boundary conditions on the liquid side of the heater are used to account for the hydrodynamic processes that occur. As shown in Fig. 2, the boiling surface can be thought of as having three different types of regions: (a) adiabatic regions inside the annular meniscus regions where active cavities reside, (b) meniscus regions around each active cavity, and (c) the remaining region having the liquid macrolayer over it. The boundary conditions are discussed below.

Heater top surface, S_t (z = H):

Portions of surface S_t that have a meniscus over them lose heat directly as a result of meniscus evaporation. The heat loss owing to meniscus evaporation will be included as part of the boundary conditions. This can be written mathematically as follows.

For all (x,y,H) ∈ any $R_{e,i}$ where i=1,..,N

if the site i is inactive, test to see if the site has activated

$$T_{act}(L_{c,i}) < \frac{\oint_{R_{c,i}} T(x,y,H,t)\, da}{\oint_{R_{c,i}} da} \quad . \tag{11}$$

If it has activated, define

$$q_{loss,i}(x,y,H,t) = -k \frac{\partial T(x,y,H,t)}{\partial z} \approx q_{meniscus,i} \tag{12a}$$

$$\approx \frac{\int_{w_i}^{f_i} h_{e,i}(T - T_{sat})da}{A_{e,i}} \approx \frac{h_{fg} m_e (T - T_{sat}) L_{s,i}}{A_{e,i}} \quad , \tag{12b}$$

where $h_{e,i}$ = the effective heat transfer coefficient for the meniscus region around the i-th site and m_e = the average effective triple-point coefficient.

If the site is active, at the beginning of a new bubble period test to see if it remains active.

$$\frac{\oint_{R_{c,i}} T(x,y,H,n\tau)\, da}{\oint_{R_{c,i}} da} > T_{deact}(L_{c,i}) \quad . \tag{13}$$

If the site remains active, continue using Eqs. (12) for all (x,y,H) ∈ $R_{e,i}$.

Bottom Surface, S_b (z = 0):

The boundary condition on the bottom surface depends on the type of heating method used. The general boundary condition can be written as

$$(1-\zeta)\, q_{input}(x,y,0,t) = -k\, \frac{\partial T(x,y,0,t)}{\partial z} \quad . \tag{14}$$

For ohmic heating ($\zeta = 1$), the bottom boundary condition becomes

$$\frac{\partial T(x,y,0,t)}{\partial z} = 0 \quad . \tag{15}$$

If externally heated ($\zeta = 0$), the bottom boundary condition becomes

$$q_{input}(x,y,0,t) = -k\, \frac{\partial T(x,y,0,t)}{\partial z} \quad . \tag{16}$$

Side Surfaces, S_S:

As noted earlier, the segment to be modeled includes enough nucleation sites to be representative of the region under the mushroom bubble. Thus, the sides of the heater segment being considered are assumed to be insulated (symmetry boundary conditions) so that

$$\frac{\partial T(x,y,z,t)}{\partial \eta} = 0 \quad , \tag{17}$$

where η is the normal to the side surface.

Macrolayer boundary conditions

The top surface of the macrolayer and the vertical walls of the vapor stems in the macrolayer are assumed to be at the saturation temperature.

$$T|_{S_{mt}} = T_{sat} \quad , \tag{18a}$$

and

$$T|_{S_{mv,i}} = T_{sat} \quad , \tag{18b}$$

where subscript i refers to all active sites.

Temporal constraints

Initial condition (t = 0):

An initial temperature distribution is specified:

$$T(x,y,z,0) = \begin{cases} T_i(x,y,z) \text{ for } 0 \le z \le H \\ T_{sat} \text{ for } H < z \le H+\delta \end{cases} . \tag{19}$$

Conditions at the beginning of each period ($t = m\tau$, for all positive integers m):

Periodic temporal conditions are imposed on the macrolayer by the liquid-resupply mechanism associated with the mushroom bubble departure. The thickness of the macrolayer is reset after each hovering period,

$$\delta(m\tau) = \delta_i , \tag{20}$$

where δ_i is prescribed by the following equation proposed by Haramura and Katto (1983),

$$\delta_i = \frac{\pi}{2}\sigma\left(\frac{\rho_f+\rho_g}{\rho_f\rho_g}\right)\left(\frac{A_v}{A_h}\right)^2\left(\frac{\rho_g h_{fg}}{q}\right)^2 . \tag{21}$$

The temperature profile in the macrolayer is reset after each hovering period to conform with the assumption that fresh saturated liquid is supplied to the near-surface region each time the overlying vapor mushrooms departs.

$$T(x,y,z,m\tau) = T_{sat} , \text{ for } H < z \le H+\delta . \tag{22}$$

This also causes a quench of the surface, so that

$$T(x,y,H,m\tau) = T_{contact} , \tag{23}$$

where $T_{contact}$ is the contact temperature for two semi-infinite media brought together.

The bubble's hovering period, τ, is calculated using the equation of Haramura and Katto (1983),

$$\tau_d = \left(\frac{3}{4\pi}\right)^{1/5}\left[\frac{4\left(\frac{11}{16}\rho_f+\rho_g\right)}{g(\rho_f-\rho_g)}\right]^{3/5}\left(\frac{A_h q}{\rho_g h_{fg}}\right)^{1/5} . \tag{24}$$

Macrolayer thinning

The heat dissipated from the heater as a result of conduction to the macrolayer and by evaporation of menisci are assumed to contribute toward one-dimensional thinning of the macrolayer. Thus, the top surface of the macrolayer is a moving boundary. The thinning of the macrolayer can be written as

$$-h_{fg}A_{mt}\rho_f\frac{d\delta}{dt}=k\int_{S_{mt}}\left.\frac{dT}{dz}\right|_{z=H+\delta}+\sum_i\left[k\int_{S_{mv,i}}\frac{dT}{d\eta}da+\int_{R_{e,i}}q_{loss,i}da\right], \tag{25}$$

where the summation is over all active sites on the surface.

Having discussed the details of the heat transfer model, we will now look at the numerical implementation of the model.

NUMERICAL MODEL

The present study uses a finite volume discretization scheme for solving the system described in the previous sections. Integration of the fundamental form of the governing equation [Eq. (1)] over a control volume V_j, and application of the divergence theorem yields the following equation for a lumped parameter representation of the evolution of the temperature over that control volume.

$$\left(V\rho C_p\right)_j\frac{T_j^{n+1}-T_j^n}{\Delta t}=\sum_{i=1}^{n_j+2}A_ik_i\frac{T_i-T_j}{\Delta x_i}+q'''V_j\ . \tag{26}$$

Subscript j refers to the control volume under consideration and subscript i refers to the lumped quantities in each of the neighboring elements of node j. Δx_i is the distance between the center of element j and that of its neighboring element i. Node j has n_j coplanar neighbors and two axial neighbors. The second term on the right-hand side is a source term that accounts for the boundary conditions as well as possible internal generation as a result of ohmic heating.

Determination of the temperature distribution of the system at any time thus reduces to two steps:

(a) discretize the domain into a sufficient number of control volumes, and

(b) march the solution forward in time by solution of the system of equations described by Eq. (26) for all the control volumes in the domain.

The domain geometry changes at each time step as a result of macrolayer evaporation and possible cavity activation. The new macrolayer height is determined using the discretized form of Eq. (25). The number of levels in the macrolayer can be reduced at any time step during the hovering period if necessary. This feature has been incorporated to prevent the reduction of the macrolayer control volume heights to extremely small values when the macrolayer thickness becomes very small. If the initial thickness of the macrolayer is sufficiently small at the beginning of the hovering period, the macrolayer may dry out completely during a period. If this occurs, the heater surface is assumed to be adiabatic for the remainder of the period, and the problem domain is confined to the heater alone. Possible cavity activation and when it occurs has been discussed previously.

Step (b) is repeated for successive hovering periods until either a stationary solution with subharmonic of order 1 is obtained or a specified number of bubble hovering periods have occurred. A stationary solution with subharmonic of order 1 is defined to be where the area- and period-averaged values of the surface temperature are within a specified tolerance level of the corresponding value for the previous period. Whereas the code does not check for it, a stationary solution with subharmonic of order n would show the area- and period-averaged values of the surface temperature to repeat in proper sequence every n bubble lifetimes. In general, stationary solutions for the heater side characteristics are not guaranteed.

Steps (a) and (b) are discussed in the following sections.

DISCRETIZATION

The control volumes used in the present study are prismatic with polygonal cross sections. The polygons can be regular hexagons or a set of irregular polygons. From a computational point of view, the regular hexagons are more efficient since they generate longer computational vectors. However, the irregular polygons are preferred in cases where complex boundaries are to be considered.

In the axial direction, the heater and macrolayer are divided into a number of slabs, the heights of which can be varied from one level to the next.

The mesh is generated from a Delaunay triangulation (Voronoi tessellation) of the full cross-sectional area of the problem domain. The polygons that make up the Voronoi diagram have the property that every point on the common edge (the Voronoi edge) of two adjacent polygons is equidistant from the centers of the polygons. Also, the line connecting the centers of the adjacent polygons is normal to the Voronoi edge. The granularity and regularity of the mesh can be tailored to the requirements of the problem by suitable definition of the seed points used to generate the polygons.

The cross-sectional discretization is dictated by the physical constraints of the problem. As mentioned earlier, the energy loss from the heater by meniscus evaporation is confined to a small region along the periphery of the vapor stems. This places natural limits on the dimensions of the polygons in the region near the stems. An example of the lateral discretization scheme is shown in Fig. 4. The vertical discretization scheme in the neighborhood of the vapor stem bases is shown in Fig. 5. Larger polygons are employed in regions far from the vapor stem locations.

The initial thickness of the macrolayer is typically between 50 and 100 μ for heat fluxes of interest. To ensure sufficient resolution of temperature gradients in this region, the macrolayer thickness is divided into a minimum of six levels. A numerical study [see Sadasivan et al. (1993c)] on the optimum discretization scheme for the problem under consideration indicated that to ensure a smooth transition to the heater region, a correspondingly high axial grid point density is required near the heater surface. The height of the surface control volumes is set to values on the order of 5 μ. Heights of control volumes in lower levels in the heater are increased cumulatively by a factor of two or less as the overall thickness allows.

SOLUTION

The problem domain consists of all the control volumes that represent liquid or solid. The control volumes that represent the vapor stems are flagged suitably and are eliminated from consideration. The set of energy balance statements

[Eq. (26)] written for each relevant control volume in the problem domain using an implicit or semi-implicit time stepping scheme comprises a sparse linear system.

For typical lateral discretization schemes using irregular polygons, the coefficient matrix of the linear system is unsymmetric. Further, because of the large difference in thermal properties between the liquid and heater control volumes, the matrix often is moderately ill-conditioned. This will be discussed later.

A number of conjugate-gradient-like methods for unsymmetric systems were tested on a sample problem to investigate the convergence characteristics as well as computational costs (see Sadasivan et al. (1993b) for more detail). The sample problem is as follows. A square heater of thickness 50 μ is divided into 6 axial levels with the thickness of the surface level being 5 μ and increasing in 1-μ steps to a value of 10 μ for the lowest level. The macrolayer initially is 98 μ thick and is divided into 10 levels. Other problem specification parameters such as input heat flux are assigned values consistent with typical experimental values.

The convergence characteristics of various schemes were compared. The conjugate-gradient-squared (CGS) scheme with different preconditioning approaches was found to be better than other schemes such as ORTHOMIN. Among the different preconditioning methods tested, the overlaxed Jacobi-preconditioned CGS method was found to be the best compromise between good convergence characteristics and economical computational costs. This method has been used in the present study.[1]

The eigenvalue spectrum of the coefficient matrix was evaluated; the spectral condition number ranged from 10^2 to 10^4 depending on a number of problem specification parameters. Coarser axial discretization in the heater results in a lower condition number. However, as has been pointed out earlier, the discretization scheme in the heater has to be relatively fine in the region near the surface so as to resolve the temperature gradients near the heater-macrolayer interface. The condition number increases as the time step size is increased.

[1]MACRO3D contains appropriate provisions to select other solution methods in the event of a breakdown.

PROGRAM VALIDATION AND NUMERICAL ERRORS

The use of a lumped-parameter approach results in a conservative estimate of surface temperature. Ball (1976) indicated more accurate results can be obtained by using small values Δx and/or larger values of Δt. A number of tests were done to assess the accuracy and validity of results obtained using MACRO3D, and to arrive at spatial and temporal grid sizes that ensure size-independence. For purposes of brevity, the details of rationale for selecting the optimum nodalization scheme and time steps are referred to previous reports [Sadasivan et al. (1993a,c)]. A brief overview of the validation process is provided below.

In a typical boiling situation, the thickness of the macrolayer is on the order of tens of microns. To ensure a smooth transition to the liquid region from the heater region, the control volumes near the top surface of the heater must also be correspondingly small. Calculations were made using different values of the height of the heater surface control volumes. The results indicate that a height of 10 μ, or lower, for the surface control volumes ensures grid-independent solutions. The heights of the control volumes in the lower levels of the heater are incremented by a factor of two in the downward direction.

A number of tests were also made to verify the influence of cross-sectional discretization. Because of the relatively small dimensions of the stems, the Delaunay mesh has to be necessarily fine in the stem regions (portions of the heater surface below potential stem locations). The granularity of the mesh can be increased gradually in regions away from the stems. Test problems were solved for different mesh granularity in the stem regions as well as in the macrolayer-covered regions. It was found that the results are relatively insensitive to the stem and macrolayer-region granularities.

The results were found to be sensitive to the dimension of the control volumes along the periphery of the stems. This is because the current model assumes that active stems participate in heat transer by direct dissipation of heat from the surface control volumes located on the periphery of the stems. Thus the dimensions of the meniscus control volumes would be dictated by the physical characteristics of the meniscus. Studies by Wayner et al. (1976) and others indicate that the bulk of the heat transfer occurs in the evaporating thin-film region of the meniscus, the width of which is in the range of 10 to 30 μ. The

radial dimensions of the control columns on the stem periphery are assigned values in this range. The average surface temperature results vary less than 0.3 K within this range. This is accepted as a reasonably small error.

MACRO3D was used, with appropriate modifications, to solve simple conduction test problems with analytical solutions. Benchmark problems considered variety of boundary conditions and dimensions. The code-calculated results were in excellent agreement with the analytical results.

Simple transient conduction problems were solved to ensure that there were no errors in the coding process that led to spurious heat sources or sinks. The transient cooling of a thin copper slab with specified initial temperature distribution, and subject to unform convective cooling on one surface, and uniform heat flux on another surface can be solved using conventional Laplace transform techniques. This analytical solution was compared with results obtained using MACRO3D. The results showed good agreement.

Transient conduction problems were also solved using MACRO3D and the commercial analysis code, ABAQUS; comparison of the results indicated good agreement. This assures the correctness and validity of the scheme and approach used in MACRO3D.

The present calculations were carried out on Cray supercomputers that have a roundoff error on the order of 10^{-14} in the single-precision mode, and 10^{-29} in double-precision mode. The effect of roundoff error was assessed using a comparison of results using single-precision and double-precision arithmetic. For a typical sample problem considered, the results differed in the tenth significant digit over a single bubble lifetime, i.e., less than 10^{-6} K. While this is an acceptably small roundoff error, it is important to realize that roundoff error may ultimately dominate the long term behavior of a nonlinear problem.

For a typical problem tested, MACRO3D was found to run about seven times faster in vector mode than in scalar mode. This confirms that the code is highly vectorized.

SUMMARY

This paper described the formulation and numerical implementation of a model aimed at investigating various aspects of high heat flux nucleate boiling. It has

been tested extensively using a number of test problems. The model and code will be used to investigate nonlinear aspects of high heat flux boiling heat transfer. Results are presented in a companion paper (Part II. Results).

NOMENCLATURE

A	area [m^2]
C_p	specific heat [J/kg°C]
$g(x,y,z,t)$	function representing cavity perimeter function
$f(x,y,z,t)$	function
H	heater thickness [m]
h_{fg}	heat of evaporation [J/kg]
h_e	heat transfer coefficient in the meniscus region [$W/m^2°C$]
k	thermal conductivity [W/m°C]
L	perimeter [m]
m	number of hovering periods
m_e	triple-point evaporation coefficient [kg/ms°C]
q'''	heat generation rate [W/m^3]
R	radius [m]
S	surface
T	temperature [°C]
t	time [s]
V	volume [m^3]
x,y,z	Cartesian coordinates

Greek

ρ	density [kg/m^3]
σ	surface tension [kg/s^2]
δ	macrolayer thickness [m]
ξ	heat input flag
τ	hovering period [s]
Δx	distance between the centers of neighboring cells [m]
η	normal to surface

Subscripts

act	activation
b	bottom
c	cavity
c,i	cavity for i-th cell
contact	liquid-solid interface
deact	deactivation
e	meniscus region
g	vapor
loss	heat loss from a cell
i	i-th cell or cavity
m v	vertical wall of vapor stem
m t	top surface of macrolayer
sat	saturation
s	side
SA	surface averaged
t	top

ACKNOWLEDGMENT

This work would not have been possible without earlier efforts by Drs. K. O. Pasamehmetoglu and P. Chappidi as post-doctoral members of Los Alamos National Laboratory.

REFERENCES

Ball, S. J., 1976, "ORECA-I: A Digital Computer Code for Simulating the Dynamics of HTGR Cores for Emergency Cooling Analysis," Oak Ridge National Laboratory report ORNL/TM-5159.

Calka, A., and Judd, R. L., 1985, "Some Aspects of the Interaction Among Nucleation Sites During Saturated Nucleate Boiling," *Int. J. Heat Mass Transfer* **28**, pp. 2331–2342.

Chekanov, V.V., 1977, "Interaction of Centers in Nucleate Boiling," Translated from *Teplofizika Vysokikh Temperatur* **15** (1), pp. 121–128.

Dhir, V. K., 1990, "Nucleate and Transition Boiling Heat Transfer Under Pool and External Flow Conditions," Proceedings of 9th International Heat Transfer Conference, Vol. 1, pp. 129–155.

Griffith, P., and Wallis, J. D., 1960, "The Role of Surface Conditions in Nucleate Boiling," Chem. Engr. Prog. Symp. Ser., Vol. 56, pp. 49–62.

Haramura, Y., and Katto, Y., 1983, "A New Hydrodynamic Model of Critical Heat Flux, Applicable Widely to Both Pool and Forced Convection Boiling on Submerged Bodies in Saturated Liquids," *Int. J. Heat Mass Transfer* **26**(3), pp. 389–399.

Hsu, Y. Y., 1962, "On the Size Range of Active Nucleation Cavities on a Heating Surface," *J. Heat Transfer* **84**, pp. 207–216.

Kenning, D. B. R., 1990, "Wall Temperatures in Nucleate Boiling: Spatial and Temporal Variations," Proc. 9th Int. Heat Transfer Conf., Jerusalem, Vol. 3, pp. 33–38.

Kenning, D. B. R., 1992, "Wall Temperature Patterns in Nucleate Boiling," *Int. J. Heat and Mass Transfer* **35**, pp. 73–86.

Moon, F. C., 1987, Chaotic Vibrations, John Wiley and Sons, New York, pp. 104–107.

Pasamehmetoglu, K. O., and Nelson, R. A., 1991, "Cavity-to-Cavity Interaction in Nucleate Boiling: the Effect of Heat Conduction Within the Heater," AIChE Symp. Ser., No. 282, Vol. 87, pp. 342–351.

Pasamehmetoglu, K. O., Chappidi, P. R., Unal, C., and Nelson, R. A., 1993, "Saturated Pool Nucleate Boiling Mechanisms at High Heat Fluxes," *Int. J. and Heat Mass Transfer* (in press).

Sadasivan, P., Unal, C., and Nelson, R. A., 1993a, "MACRO3D—A Three-Dimensional Finite Volume Computer Code for the Analysis of High Heat-Flux Nucleate Boiling," Los Alamos National Laboratory document LA-UR-93-1835.

Sadasivan, P., Unal, C., and Nelson, R. A., 1993b, "Iterative Methods for Solving Sparse Unsymmetric Linear Systems," Los Alamos National Laboratory document LA-UR-93.

Sadasivan, P., Unal, C., and Nelson, R. A.,, 1993c, "MACRO3D—Discretization Schemes for Slender Geometries," Los Alamos National Laboratory document LA-UR-93-3233.

Sultan, M. and Judd, R. L., 1983, "Interaction of Nucleation Phenomena at Adjacent Sites in Nucleate Boiling," Trans. ASME, *J. Heat Transfer* **105**, pp. 3–9.

Wayner, P. C., Kao, Y. K., and laCroix, L. V., 1976, "The Interline Heat Transfer Coefficient of an Evaporating Vapor Film," *Int. J. Heat Mass Transfer* **19**, pp. 487–492.

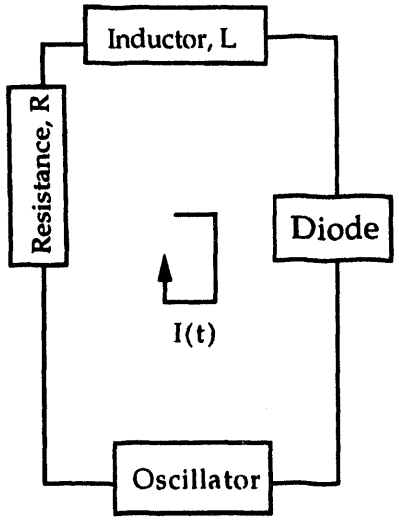

Fig. 1. Sketch of a diode circuit that exhibits chaotic oscillations [from Moon (1987)].

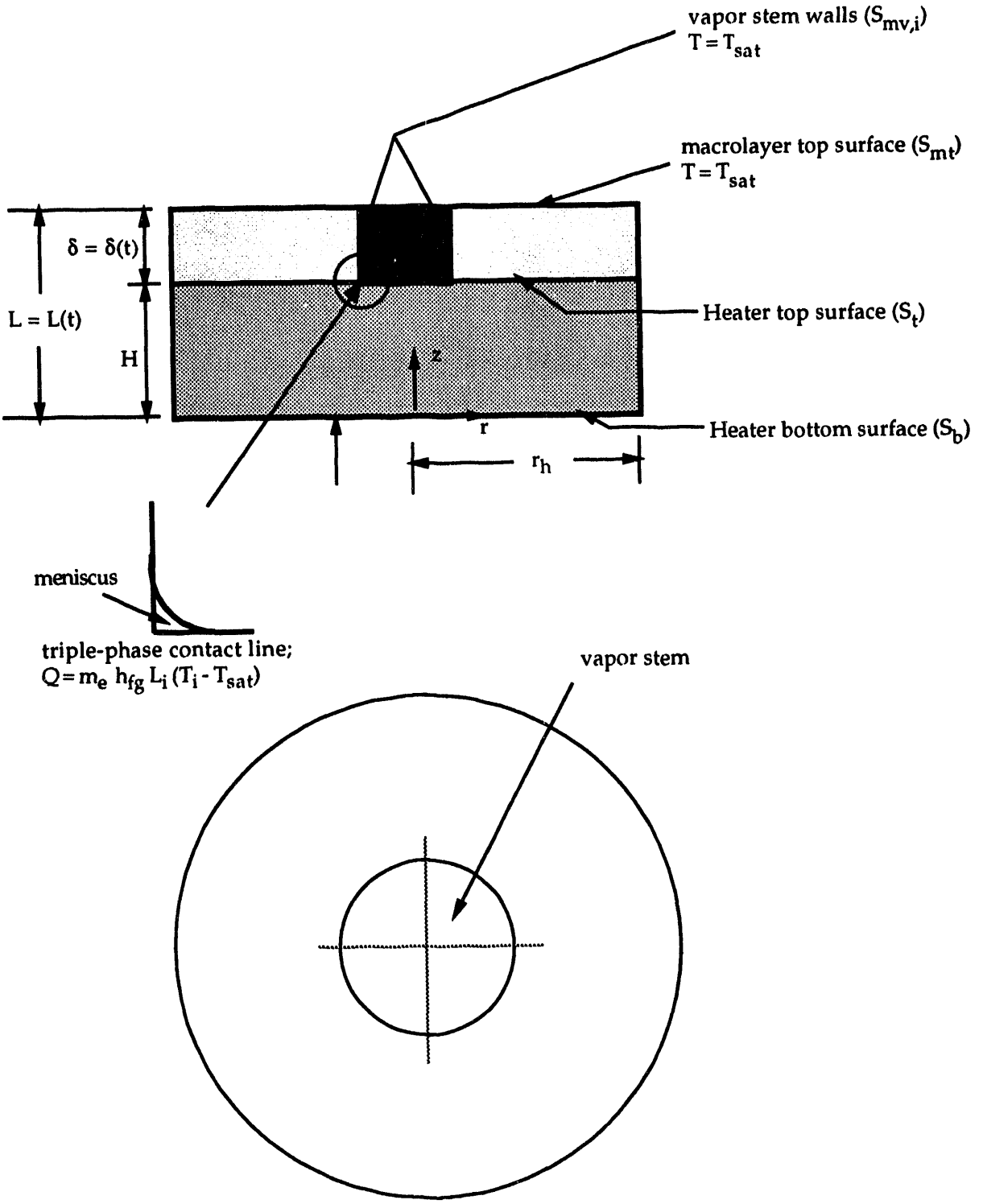

Fig. 2. Sketch of macrolayer-heater configuration and boundary conditions (For purposes of clarity, only one stem is shown in the macrolayer).

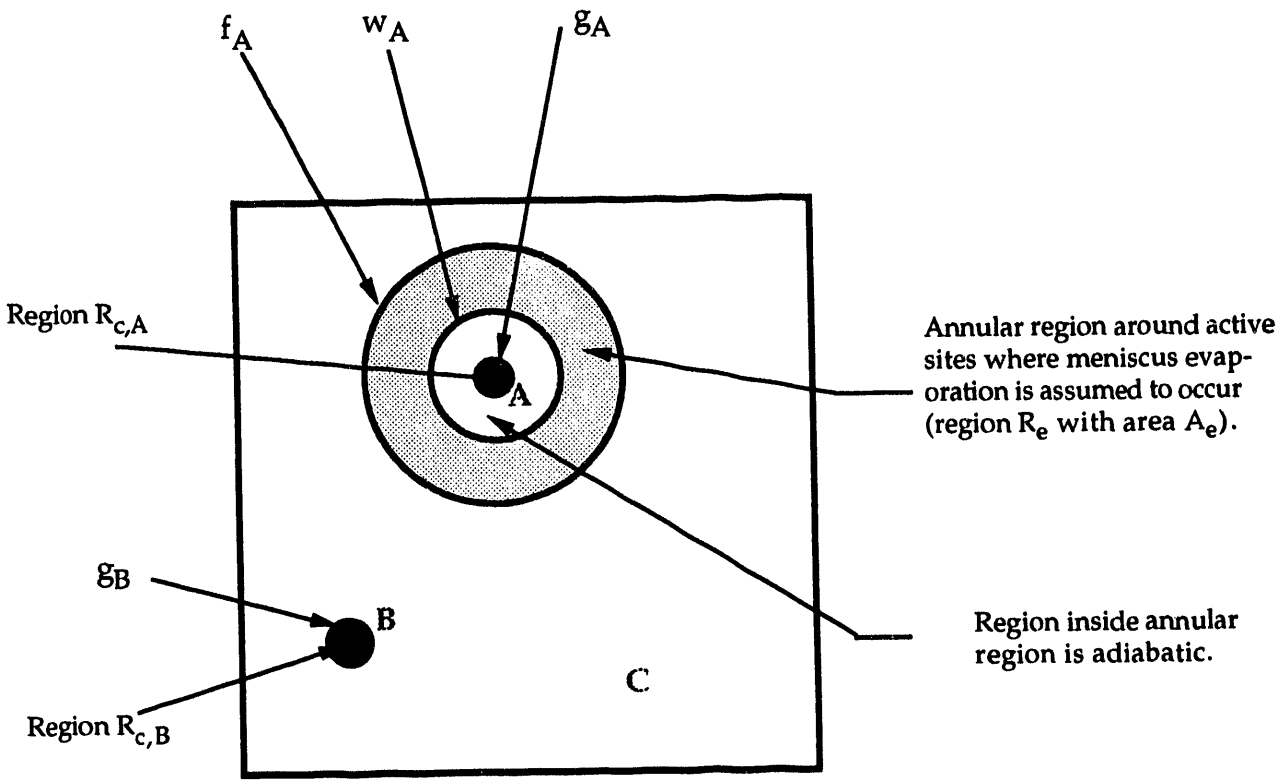

A: Active site with associated stem/meniscus
B: Inactive site (in contact with liquid macrolayer)
C: Heater surface (in contact with liquid macrolayer)

Fig. 3. Sketch of a portion of the heater surface, shown enlarged to indicate the geometric parameters associated with an active site.

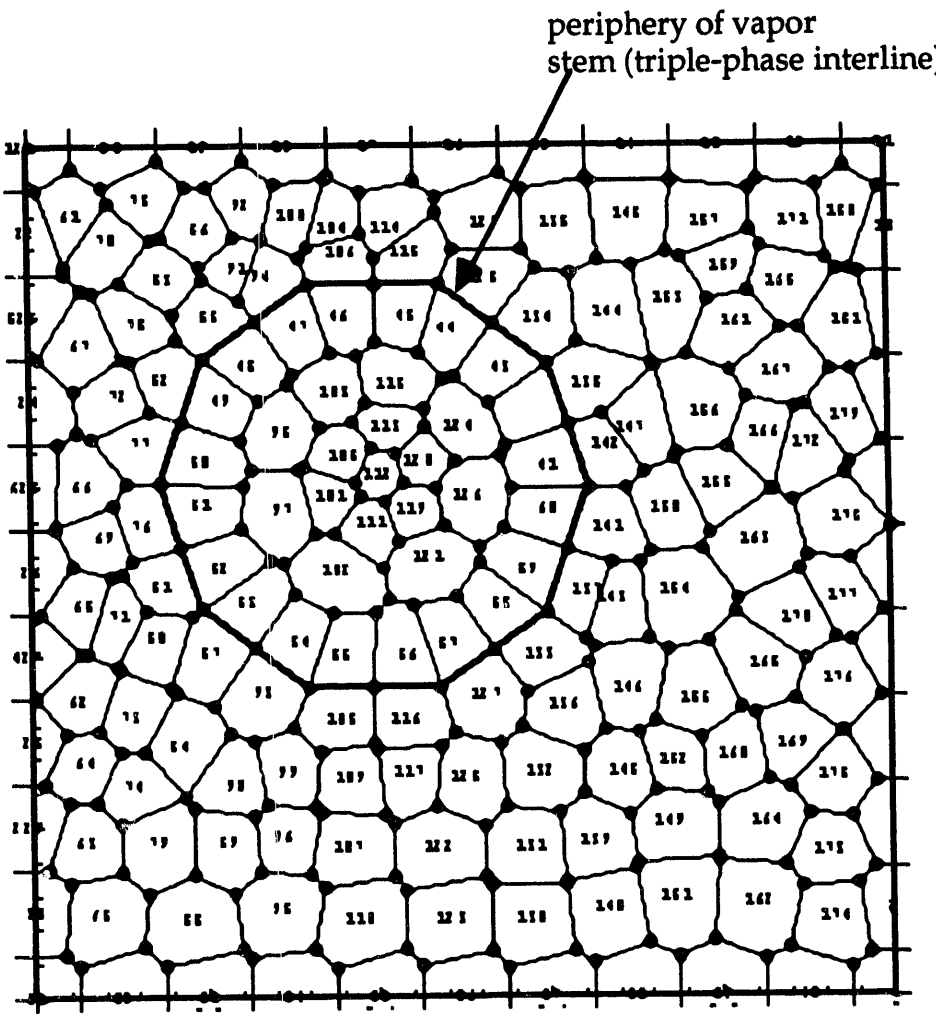

Fig. 4. Example of the lateral discretization scheme (A portion of the heater surface with one active vapor stem is shown. The surface control volumes along the concave side of the triple-line interface dissipate heat as a result of meniscus evaporation. The numbers denote the cell numbers).

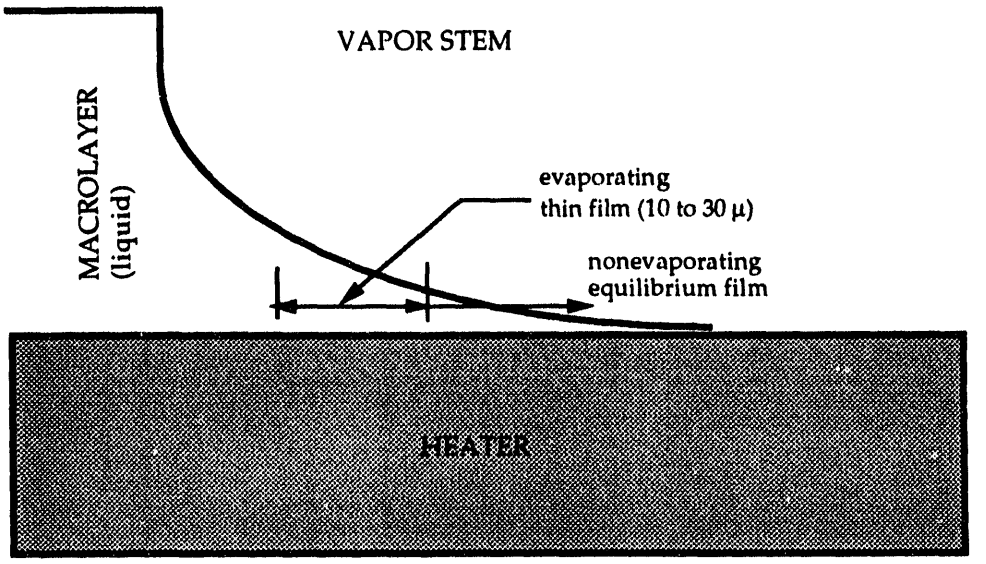

(a)

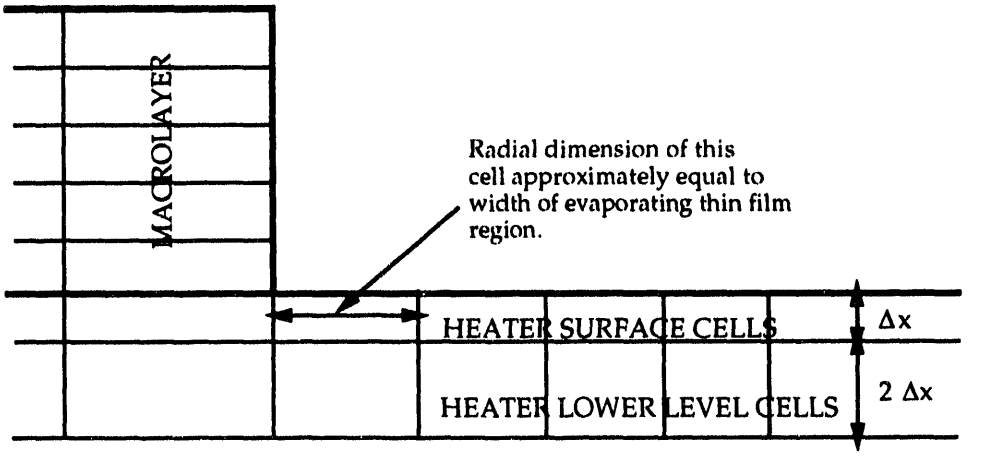

(b)

Fig. 5. (a) Sketch of triple interface contact region and meniscus and (b) corresponding discretization scheme in the heater (only the topmost two levels shown).

DATE
FILMED
10/5/94

END